HHS Public Access

Author manuscript

Mol Psychiatry. Author manuscript; available in PMC 2024 September 01.

Published in final edited form as:

Mol Psychiatry. 2024 March ; 29(3): 624–632. doi:10.1038/s41380-023-02353-z.

Unique pharmacodynamic properties and low abuse liability of the μ-opioid receptor ligand (S)-methadone

Marjorie R. Levinstein[1,†], **Paulo A. De Oliveira**[2,†], **Nil Casajuana-Martin**[3,†], **Cesar Quiroz**[2], **Reece C. Budinich**[1], **Rana Rais**[4], **William Rea**[2], **Emilya N. Ventriglia**[1], **Natàlia Llopart**[5], **Verònica Casadó-Anguera**[5], **Estefanía Moreno**[5], **Donna Walther**[6], **Grant C. Glatfelter**[6], **David Weinshenker**[7], **Carlos A. Zarate Jr.**[8], **Vicent Casadó**[5], **Michael H. Baumann**[6], **Leonardo Pardo**[3], **Sergi Ferré**[2,*], **Michael Michaelides**[1,9,*]

[1]Biobehavioral Imaging and Molecular Neuropsychopharmacology Unit, National Institute on Drug Abuse Intramural Research Program, Baltimore, MD 21224 USA

[2]Integrative Neurobiology Section, National Institute on Drug Abuse Intramural Research Program, Baltimore, MD 21224 USA

[3]Laboratory of Computational Medicine, Biostatistics Unit, Faculty of Medicine, Universitat Autònoma Barcelona, Bellaterra, 08193 Barcelona, Spain

[4]Johns Hopkins Drug Discovery, Neurology and Pharmacology, Johns Hopkins School of Medicine, Baltimore, MD, 21205, USA

[5]Laboratory of Molecular Neuropharmacology, Department of Biochemistry and Molecular Biomedicine, Faculty of Biology and Institut de Biomedicina de la Universitat de Barcelona, 08028 Barcelona, Spain

[6]Designer Drug Research Unit, Intramural Research Program, National Institute on Drug Abuse, National Institutes of Health, Baltimore, MD 21224 USA

[7]Department of Human Genetics, Emory University School of Medicine, Atlanta, GA 30322 USA

[*]Corresponding authors: Sergi Ferré, M.D., Ph.D., sergi.ferre@nih.gov, Michael Michaelides, Ph.D., mike.michaelides@nih.gov.
[†]These authors contributed equally

Author Contributions

Designed and performed experiments, analyzed data, and wrote the manuscript: MRL, PADO, MHB
Designed experiments, analyzed data, and wrote the manuscript: SF, MM
Designed and performed experiments, analyzed data: CQ, RR, VCA
Performed experiments and analyzed data: WR, NL, D Walther
Performed computational models, analyzed data and wrote the manuscript: NC, LP
Designed experiments and analyzed data: EM, VC
Performed experiments: ENV, RCB, GCG
Contributed resources and reagents and contributed to writeup of the paper: D Weinshenker, CAZ
All coauthors reviewed the manuscript and provided comments.

Competing Interests

MM has received research funding from AstraZeneca, Redpin Therapeutics, and Attune Neurosciences. Dr. Zarate is a full-time U.S government employee. He is listed as a coinventor on a patent for the use of ketamine in major depression and suicidal ideation. Dr. Zarate is listed as a coinventor on a patent for the use of (2R,6R)-hydroxynorketamine, (S)-dehydronorketamine and other stereoisomeric dehydro and hydroxylated metabolites of (R,S)-ketamine metabolites in the treatment of depression and neuropathic pain. Dr. Zarate is listed as co-inventor on a patent application for the use of (2R,6R)-hydroxynorketamine and (2S,6S)-hydroxynorketamine in the treatment of depression, anxiety, anhedonia, suicidal ideation and post-traumatic stress disorders. Dr. Zarate has assigned his patent rights to the U.S. government but will share a percentage of any royalties that may be received by the government.

[8]Section on the Neurobiology and Treatment of Mood Disorders, National Institute of Mental Health Intramural Research Program, Bethesda, MD 20892 USA

[9]Department of Psychiatry and Behavioral Sciences, Johns Hopkins University School of Medicine, Baltimore, MD 21205 USA

Abstract

(R,S)-methadone ((R,S)-MTD) is a μ-opioid receptor (MOR) agonist comprised of (R)-MTD and (S)-MTD enantiomers. (S)-MTD is being developed as an antidepressant and is considered an N-methyl-D-aspartate receptor (NMDAR) antagonist. We compared the pharmacology of (R)-MTD and (S)-MTD and found they bind to MORs, but not NMDARs, and induce full analgesia. Unlike (R)-MTD, (S)-MTD was a weak reinforcer that failed to affect extracellular dopamine or induce locomotor stimulation. Furthermore, (S)-MTD antagonized motor and dopamine releasing effects of (R)-MTD. (S)-MTD acted as a partial agonist at MOR, with complete loss of efficacy at the MOR-galanin (Gal1) receptor heteromer, a key mediator of the dopaminergic effects of opioids. In sum, we report novel and unique pharmacodynamic properties of (S)-MTD that are relevant to its potential mechanism of action and therapeutic use.

One-sentence summary

(S)-MTD, like (R)-MTD, binds to and activates MORs in vitro, but (S)-MTD antagonizes the MOR-Gal1R heteromer, decreasing its abuse liability.

Keywords

opioid; computational model; NMDAR

Opioid medications are potent and efficacious analgesics, but their use can be associated with serious adverse effects such as tolerance, dependence, and respiratory depression. (R,S)-methadone ((R,S)-MTD) is an opioid medication used as an analgesic and a maintenance therapy for opioid use disorder (OUD) [1, 2]. (R,S)-MTD is a long-acting μ-opioid receptor (MOR) agonist that is comprised of equal amounts of (R)-MTD and (S)-MTD enantiomers. The therapeutic properties of (R,S)-MTD are believed to be mediated by the pharmacological actions of (R)-MTD [3], which is also prescribed alone as a maintenance therapy for OUD[4].

(S)-MTD, historically considered the inactive enantiomer of (R,S)-MTD, is now under clinical development as a treatment for depression[5–7]. Although its precise *in vivo* pharmacology is not well understood, (S)-MTD's antidepressant mechanism of action is attributed to N-methyl-D-aspartate receptor (NMDAR) antagonism[5–9]. Specifically, (S)-MTD has ~2.6–7.4 μM affinity at NMDARs[10] and produces behavioral and neurochemical effects in rodents that are similar to those produced by ketamine[6, 7], a known NMDAR antagonist and effective antidepressant. However, recent evidence implicates MOR agonism as a relevant mechanism for ketamine's antidepressant effects, its abuse liability, and *in vivo* pharmacology[11–14]. Furthermore, (S)-MTD's affinity for the MOR is ~300 times greater

than its affinity for the NMDAR[10, 15]. Finally, (S)-MTD is an established MOR agonist, whereas its NMDAR actions involve noncompetitive antagonism[10].

(R,S)-MTD and its enantiomers are classified as Schedule II controlled substances by the United States Drug Enforcement Administration (DEA). Nevertheless, (R,S)-MTD produces weaker activation of midbrain dopamine systems and has lower abuse liability when compared to other opioids[16]. The reduced dopaminergic effects of (R,S)-MTD are dependent on its unique, weak interaction with MOR-galanin 1 receptor (Gal_1R) heteromers specifically expressed in the ventral tegmental area (VTA). MOR-Gal_1R in the VTA are known to mediate the activation of the dopaminergic system by opioids[16], but the effects of (R) and (S) enantiomers of MTD at these heteromers are unknown.

In order to explore the analgesic and abuse liability profiles of (R,S)-MTD and its enantiomers, and to address the gaps in knowledge about these compounds, we performed an in-depth *in vitro*, *in vivo* and *in silico* pharmacological characterization of (R,S)-MTD, (R)-MTD and (S)-MTD. In contrast to prior studies, we conclusively show that (S)-MTD does not act at NMDARs at doses that produce antidepressant-like effects, analgesia, or reinforcement. We also show that despite its agonism at MOR, (S)-MTD is predicted to have low abuse liability. Additionally, we report a unique pharmacodynamic effect of (S)-MTD at the MOR-Gal_1R, distinct from that of (R)-MTD, which explains (R,S)-MTD's unique actions at the MOR-Gal_1R [16]. This finding is particularly novel as it represents a rare example of enantiomers acting in opposition at the same pharmacological target. Taken together, our findings provide a novel mechanistic explanation for the differential *in vitro* and *in vivo* properties of the enantiomers, which may impact on their clinical utility.

Results

(R)-MTD and (S)-MTD preferentially bind and activate MOR

Each enantiomer was tested for its ability to competitively inhibit binding or activity at a panel of 98 receptors and enzymes that are known targets for drugs of abuse and CNS medications. At 10 μM, (R)-MTD inhibited binding at several receptors (Fig. 1A), while at 100 nM, (R)-MTD inhibited binding only at MOR (98%) and SERT (68%). At 10 μM, (S)-MTD inhibited binding at several receptors, while at 100 nM, (S)-MTD inhibited binding only at MOR (79%). We derived each enantiomer's affinity at MOR or NMDAR by measuring the binding of [^{3}H]DAMGO or [^{3}H]MK-801, respectively, in rat brain tissue. The Ki values obtained for MOR were 15.6 ± 0.1 nM for (R,S)-MTD, 7.5 ± 0.1 nM for (R)-MTD, and 60.5 ± 0.1 nM for (S)-MTD (Fig. 1B). The Ki values for NMDAR were higher – 1.96 ± 0.07 μM for (R,S)-MTD, 1.44 ± 0.07 μM for (R)-MTD, and 2.73 ± 0.07 μM for (S)-MTD (fig. S1) and approximated the Ki values reported in prior work[10].

Agonist-stimulated [^{35}S]GTPγS autoradiography in rat brain sections was used to examine the ability of (R,S)-MTD and its enantiomers to activate MOR (Fig. 1C). At 100 nM, only (R)-MTD increased [^{35}S]GTPγS recruitment in the caudate putamen (CPu) (171%) and nucleus accumbens (NAc) (151%) (Fig. 1D, E). By contrast, at 1 μM all drugs increased [^{35}S]GTPγS recruitment in CPu (R,S: 199%; R: 270%; S: 144%) and NAc (R,S: 145%; R: 164%; S: 120%) (Fig. 1D, E). At the 1 μM concentration, (R)-MTD showed significantly

greater [^{35}S]GTPγS recruitment compared to (R,S)-MTD ($P = 0.01$) and (S)-MTD ($P < 0.001$) in CPu. Additionally, (R,S)-MTD showed greater [^{35}S]GTPγS recruitment compared to (S)-MTD ($P = 0.028$). Finally, the regional distribution of (S)-MTD-induced (1μM, Fig. 1C) and (R)-MTD-induced (100 nM, fig. S1) [^{35}S]GTPγS recruitment was blocked by naloxone (10 μM) indicating opioid receptor involvement.

(S)-MTD exhibits similar analgesic efficacy as (R)-MTD and (R,S)-MTD

We next evaluated analgesic, cataleptic, and hypothermic effects in the same rats. In the hotplate, (R,S)-MTD, (R)-MTD, and (S)-MTD demonstrated full agonistic activity, with ED_{50} values (%MPE, maximum possible effect) of 1.2, 0.5 and 17.9 mg/kg, respectively (Figs. 2A, S2). The catalepsy score provides a measure of the motor and postural changes associated with high-dose opioid administration in rats. Unlike in the hot plate, when evaluating catalepsy score in rats, (S)-MTD behaved as a partial agonist, unable to achieve maximal cataleptic effects, even at 100 mg/kg. The high-dose effect was ~60% of the maximal cataleptic effects of both (R)-MTD and (R,S)-MTD, which were observed at 3 and 10 mg/kg, respectively (Figs. 2B, S2). The cataleptic ED_{50} values (%MPE) for (R,S)-MTD, (R)-MTD and (S)-MTD were 2.1, 0.9 and 59.4 mg/kg, respectively, which were two- to three-fold higher than their analgesic ED_{50} values. MOR agonists have biphasic effects on body temperature – at low doses these drugs tend to raise body temperature, but at high doses they produce hypothermia. For the three drugs, the maximal cataleptic effect corresponded to the minimal dose required to produce significant hypothermia (fig. S2). (S)-MTD-induced catalepsy did not observably saturate, and toxic higher doses were not employed. Overall, these experiments demonstrate a MOR agonistic profile of (S)-MTD, with a lower potency and a possibly lower intrinsic efficacy compared to (R)-MTD. Finally, (R)-MTD and (S)-MTD did not differ in their propensity to interact with efflux transporters or in relation to CYP-dependent metabolism (fig. S3), indicating that the two enantiomers would demonstrate similar metabolic profiles *in vivo*.

(S)-MTD exhibits lower abuse liability than (R)-MTD and (R,S)-MTD

There is evidence that (R,S)-MTD is self-administered in humans[17] and rats[18]. However, the intravenous self-administration (IVSA) of (R)-MTD and (S)-MTD has not been reported. Moreover, depending on the dose administered, (R,S)-MTD can have either rewarding or aversive effects in rats[19]. IVSA, the standard preclinical approach for predicting abuse liability of drugs in humans[20], was used to evaluate the reinforcing effects of (R,S)-MTD and its enantiomers in rats. First, we performed dose finding experiments to determine the dose of each drug that maintained IVSA. Rats exposed to various doses of (R)-MTD readily self-administered 50 μg/kg/infusion and consumed a maximum of ~2 mg/kg at the highest dose (fig. S4). Rats exposed to (S)-MTD never acquired IVSA, even at high unit doses, and did not show any evidence of dose response. Nevertheless, when (R)-MTD-trained rats were switched to (S)-MTD, they showed reliable IVSA at 500 μg/kg/infusion (S)-MTD. The switched rats consumed a cumulative dose of ~30 mg/kg at the highest (S)-MTD dose (fig. S4).

Next, we performed IVSA studies on another cohort of rats trained on either (R)-MTD (50 μg/kg/infusion), (R,S)-MTD (100 μg/kg/infusion), or (S)-MTD (500 μg/kg/infusion) (Fig.

2C–E). For the first 10 days of training, rats were on a fixed-ratio 1 (FR1) schedule. During this time, rats in all three groups learned to discriminate the active from inactive lever. On the 11th session, the schedule was increased to FR5 (5 presses for 1 infusion). Whereas rats trained on (R)- and (R,S)-MTD adjusted lever press rates to maintain stable infusion rates, rats trained on (S)-MTD did not. We then performed a dose response assessment of IVSA (Fig. 2F). Rats trained on (R)- or (R,S)-MTD displayed the typical inverted-U shaped dose-response curve, but rats trained on (S)-MTD showed no evidence of dose response. Rats given (R)-MTD showed peak infusion rates at 25 μg/kg, while rats given (R,S)-MTD peaked at 50 μg/kg. Notably, rats trained on (R,S)-MTD had more infusions at the peak unit dose than those on (R)-MTD, and the (R,S)-MTD curve was significantly shifted to the right indicating that larger drug amounts were required to reach the same level of reinforcement.

(R)-MTD and (S)-MTD preferentially bind to MOR *in vivo*

In order to better understand the effects of (R,S)-MTD and its enantiomers *in vivo,* we assessed their occupancy at MOR and NMDAR using doses based on drug exposure levels from the studies noted above, and prior reports on antidepressant-like doses of (S)-MTD used in rats[6, 7]. Rats were injected with saline (1 ml/kg, sc), (R,S)-MTD (4 mg/kg, sc), (R)-MTD (2 mg/kg, sc), or (S)-MTD (30 mg/kg, sc) 30 min before decapitation, blood collection, and brain extraction. Brains were split into two hemispheres. One hemisphere was used to assess drug amounts whereas the other was sectioned (20 μm) and subjected to autoradiography using [^{3}H]DAMGO or [^{3}H]MK-801 to examine occupancy at MORs or NMDARs, respectively (Fig. 2G). After 2 mg/kg of (R)-MTD, total/estimated free[22, 23] drug concentration was 640/19.2 nM ± 136/4.1 nM in plasma and 1.1/0.03 μM ± 0.15/0.005 μM in brain. After 30 mg/kg of (S)-MTD, total/free drug was 5/0.15 μM ± 0.6/0.017 μM in plasma and 11.5/0.35 μM ± 1.5/0.046 μM in brain. Finally, after 4 mg/kg of (R,S)-MTD, total/free (R)-MTD was 551/16.5 nM ± 119/3.6 nM in plasma and 1.3/0.04 μM ± 0.3/0.008 μM in brain, while total/free (S)-MTD was 580/17.4 nM ± 111/3.3 nM in plasma and 1.4/0.04 μM ± 0.3/0.009 μM in brain. The free (i.e., unbound) drug concentration provides the most accurate measure of biophase drug concentration able to engage pharmacological targets in plasma or brain[21]. Since the free concentration of (R,S)-MTD and its enantiomers is reported to be ~3% of total concentration[22, 23], it is unlikely that (R,S)-MTD or its enantiomers reach sufficient concentration to engage with NMDAR *in vivo*. By contrast, the free concentrations shown here align well with each drug's Ki at MOR. As predicted by the free concentrations of each drug, we found that 4 mg/kg (R,S)-MTD, 2 mg/kg (R)-MTD, and 30 mg/kg (S)-MTD produced near total (99%, 91%, and 79% respectively) occupancy of MORs 30 min after injection (Fig. 2H, I). Importantly, none of the drugs produced any NMDAR occupancy (Fig. 2J, K).

(R)-MTD and (S)-MTD do not produce MOR desensitization

Decreases in MOR density and desensitization contribute to the development of opioid tolerance[24]. In contrast to other MOR agonists, (R,S)-MTD does not produce tolerance, due to its ability to induce MOR internalization and recycling of re-sensitized MOR[25]. Thus, we examined to what extent repeated exposure to (R)-MTD (2 mg/kg, sc), (R,S)-MTD (4 mg/kg, sc), or (S)-MTD (30 mg/kg, sc) lead to changes in MOR density and G protein activation using [^{3}H]DAMGO and DAMGO-stimulated [^{35}S]GTPγS autoradiography. We

found that neither (R,S)-MTD nor its enantiomers produced any effect on MOR density or G protein activity (fig. S5).

Divergent pharmacodynamic effects of (R)-MTD and (S)-MTD at MOR in the VTA

In view of the apparent lower reinforcing efficacy of (S)-MTD in rats, we next examined effects of the (R,S)-MTD and its enantiomers on locomotor activity in mice. In contrast to rats, which become cataleptic following opioid exposure, mice display dose-dependent increases in locomotion[26–30]. This opioid-induced hyperlocomotion is dependent on dopaminergic activation[31–33], namely the activation of MORs expressed on GABA afferents onto VTA dopamine neurons[34]. Additionally, locomotor activation can distinguish between full and partial MOR agonists, with partial agonists producing graded increases dependent on efficacy[35]. We found that (R,S)-MTD and (R)-MTD increased locomotion, but (S)-MTD did not (Fig. 3A–D). Specifically, after 60 minutes of habituation, (R,S)-MTD produced a significant locomotor activation at 10 mg/kg (sc) but not at 3 mg/kg (sc), and 30 mg/kg (sc) was less effective than 10 mg/kg. An inverted U shape effect was also observed with (R)-MTD, which was more potent and effective at 3 mg/kg (sc). (S)-MTD did not produce any significant locomotor-activating effects, even at 100 mg/kg (sc; Fig. 3D). Moreover, when administered 15 min before (R)-MTD, (S)-MTD (10, 30 mg/kg, sc) dose-dependently counteracted the locomotor-stimulating effect of (R)-MTD (10 mg/kg, sc; Fig. 3E, F).

Repeated administration of opioids in rodents leads to psychomotor sensitization, which is classically known to depend on activation of MOR localized in the VTA[36]. We habituated mice to open-field chambers for two days before giving repeated injections of (R)-MTD (2, 5, or 10 mg/kg, ip), (R,S)-MTD (4, 10, or 20 mg/kg, ip), or (S)-MTD (20, 30, or 40 mg/kg, ip) for three days (Fig. 3G–J). (R)-MTD at 5 or 10 mg/kg and (R,S)-MTD at 10 or 20 mg/kg led to significant acute locomotion each day. Only (R)-MTD produced psychomotor sensitization at 10 mg/kg (D1 vs D2: $P = 0.01$). Mice treated with (R,S)-MTD and (S)-MTD failed to show sensitization at any dose. We also investigated whether (S)-MTD pretreatment (10 or 30 mg/kg, ip) would prevent (R)-MTD-induced (10 mg/kg, ip) sensitization (Fig. 3K, L). As before, we found that (S)-MTD dose-dependently decreased acute locomotion produced by (R)-MTD, however, it did not prevent psychomotor sensitization ((S)-MTD 0 mg/kg: D1 vs D3: $P = 0.0003$; (S)-MTD 10 mg/kg D1 vs D3: $P < 0.0001$; (S)-MTD 30 mg/kg: D1 vs D3: $P < 0.0001$).

In view of the apparent lower reinforcing efficacy of (S)-MTD in rats we next examined whether the enantiomers of (R,S)-MTD could stimulate MOR receptors in the VTA which are involved in opioid reinforcement. In particular, the weak interaction of (R,S)-MTD with MOR-Gal_1R heteromers in rat VTA is thought to underlie its reduced dopaminergic activation and lower abuse liability [16]. Thus, we studied the effects of (R)-MTD and (S)-MTD perfusion into the rat VTA, using *in vivo* microdialysis. We recently showed that the intracranial perfusion of (R,S)-MTD in the VTA was less potent and efficacious than other opioids (e.g., morphine, fentanyl and DAMGO) at eliciting somatodendritic dopamine release[16]. This reduced effect was attributed to (R,S)-MTD's weak activation of MOR-Gal_1R. Here, we show that local perfusion of (R)-MTD into the VTA produced a concentration-dependent increase in extracellular dopamine, with a significant increase at 3

μM and a larger increase at 10 μM (Fig. 3M, N), showing similar potency to that previously obtained with morphine[16]. In contrast, (S)-MTD did not induce any significant effect on extracellular dopamine levels when perfused up to 100 μM (Fig. 3N). Notably, the 100 μM concentration of (S)-MTD completely counteracted the effect of (R)-MTD on dopamine release (Fig. 3O).

In rat brain slices containing the VTA, 1 μM (R)-MTD significantly increased [^{35}S]GTPγS recruitment (121.6%, $P = 0.0003$), which was prevented by preincubation with (S)-MTD. As shown in Fig. 3P, 1 μM (S)-MTD + 1 μM (R)-MTD significantly increased [^{35}S]GTPγS recruitment (115%, $P = 0.012$), while 10 μM (S)-MTD + 1 μM (R)-MTD (107%) did not. The ability of (S)-MTD (10 μM) to reduce [^{35}S]GTPγS recruitment by (R)-MTD (1 μM) was significant ($P = 0.039$). The [^{35}S]GTPγS results also demonstrate a qualitatively different profile for (R)-MTD and (S)-MTD when comparing effects across different brain areas, with (S)-MTD showing a detectable efficacy in the striatum (Fig. 1D, E) and significantly counteracting the effect of R-MTD in the VTA, but not in the CPu or NAc (fig. S6).

Divergent pharmacodynamic effects of (R)-MTD and (S)-MTD at the MOR-Gal$_1$R heteromer

We next investigated the possibility of divergent pharmacodynamic effects MTD enantiomers at MOR-Gal$_1$R, which could explain their divergent effects on the VTA MOR. First, we evaluated possible differences in binding affinity of (R,S)-MTD, (R)-MTD, and (S)-MTD. We performed radioligand binding experiments in membrane preparations from HEK-293 cells stably transfected with human MOR alone and with human MOR-Gal$_1$R[16, 37]. The results of competitive inhibition experiments using the MOR antagonist [^{3}H]naloxone (1.7 nM) *versus* increasing concentrations of the ligands (fig. S7) were analyzed with the 'dimer receptor model' (see Methods). In both cell lines and for the three compounds, a significantly better fit was obtained for biphasic versus monophasic curves ($p < 0.05$ in all cases), indicating the preferred dimeric structure of MOR, forming heteromers or not forming heteromers with Gal$_1$R, as previously shown[37]. Table S1 shows that (R,S)-MTD, (R)-MTD and (S)-MTD bind MOR with two different affinities and negative cooperativity, both in MOR and MOR-Gal$_1$R cells. None of the obtained binding parameters show significant differences between MOR and MOR-Gal$_1$R cells for any of the ligands, indicating that the MOR-Gal$_1$R-dependent changes in the pharmacodynamic properties of (S)-MTD are not related to changes in its affinity for the MOR, but likely to its intrinsic efficacy. As expected, (S)-MTD had 14 times lower affinity than (R)-MTD in both cell types.

BRET experiments were performed to evaluate differences in the intrinsic efficacy of (R,S)-MTD, (R)-MTD and (S)-MTD at the MOR (Fig. 4A). MOR-Rluc and Gi-YFP constructs were transiently co-transfected to HEK-293T cells, and concentration-response curves of (R,S)-MTD, (R)-MTD, and (S)-MTD were analyzed for E_{max} and EC_{50} values (Fig. 4B–D). As expected, E_{max} for (S)-MTD was significantly lower than for R-MTD (about 30% lower, Fig. 4C), and EC_{50} for (S)-MTD was significantly higher than for R-MTD (about 10 times; Fig. 4D). Thus, relative to (R)-MTD, (S)-MTD is a partial and less potent MOR agonist.

CODA-RET experiments were then performed to determine whether MOR-Gal_1R heteromerization might determine the specific pharmacodynamic profile of (S)-MTD (see Methods) (Fig. 4G). HEK-293T cells were co-transfected with MOR fused to nRLuc (MOR-nRLuc), Gal_1R was fused to cRLuc (Gal_1R-cRLuc) and Gi-YFP (Fig. 4H–J). In the presence of Gal_1R, no detectable increase of response (BRET ratio) could be obtained with (S)-MTD, while the dose-response curve of (R,S)-MTD was shifted to the right, with an EC_{50} value significantly higher than for R-MTD (~10-fold; Fig. 4J). These results indicate that (S)-MTD, but not (R)-MTD, changes its pharmacological profile and loses its efficacy for the MOR when forming heteromers with Gal_1R. This implies that the changes in the pharmacological profile of (R,S)-MTD within the MOR-Gal_1R heteromer, as previously described[16, 37], depend on the modified pharmacodynamic properties of (S)-MTD. Consistent with this, increasing concentrations of (S)-MTD progressively counteracted the effect of a minimal concentration with maximal effect of (R)-MTD (10 μM) (Fig. 4K). At the highest concentration of (S)-MTD (1 mM), the effect of (R)-MTD was completely blocked, and CODA-RET measurements were not significantly different from basal values (Fig. 4L). As a control, the same design was applied with BRET experiments with the MOR alone. In this case, the highest concentration of (S)-MTD (1 mM) did not counteract the effect of (R)-MTD (10 μM) (Fig. 4E, F), and only decreased its effect to the expected maximal level of efficacy of (S)-MTD. These results, therefore, complement those obtained with *in vivo* and *ex vivo* experiments in the VTA (microdialysis and [^{35}S]GTPγS) and with locomotor activation and psychomotor sensitization in mice, and provide strong evidence for their mediation by MOR-Gal_1R heteromers.

Molecular mechanism of the MOR-Gal_1R-dependent pharmacodynamic profile of (S)-MTD

The recently reported structure of MOR in complex with fentanyl [38] can be used as a template to understand the pharmacological differences among the enantiomers of (R,S)-MTD at the molecular level. We first performed five replicas of unbiased 1 μs molecular dynamics (MD) simulations of (S)-MTD and (R)-MTD docked into the MOR monomer (see Methods). Root-mean-square deviations (rmsd) of the simulations show that the proposed docking models of (S)-MTD and (R)-MTD remained highly stable (fig. S8). In these models, the protonated amine of (S)-MTD and (R)-MTD forms the conserved ionic interaction with D149$^{3.32}$, and both phenyl groups adopt a “V” shaped conformation in the orthosteric binding site but, importantly, with significant differences (Fig. 4M, N). For (R)-MTD, both phenyl rings point up to form T-shaped aromatic interactions with H299$^{6.52}$ and W320$^{7.35}$, whereas the phenyl rings of (S)-MTD point down to interact with W295$^{6.48}$ in a “sandwich” mode, in which the aromatic Trp ring is between both phenyl rings (figs. S8–S9 show a detailed analysis of the binding modes). We suggest that the phenyl ring of (S)-MTD positioned between W295$^{6.48}$ and TM 5, absent in (R)-MTD, restricts the necessary movement of W295$^{6.48}$ for activation[38, 39], which explains the decreased ability of (S)-MTD to activate MOR.

To understand the inability of (S)-MTD to activate MOR in the presence of Gal_1R, at the molecular level, we first needed to computationally model the MOR-Gal_1R heteromer (fig. S10). Previously reported bimolecular fluorescence complementation (BiFC) and total internal reflection fluorescence (TIRF) microscopy experiments revealed that the interface

for the MOR-MOR homodimer changed from the TM 5/6 to the TM 4/5 interface in the absence or presence, respectively, of Gal_1R [37]. Thus, we hypothesized that the MOR-MOR homodimer interacting via the TM 4/5 interface disables (S)-MTD to activate MOR. To test this hypothesis, we performed five replications of unbiased 1 μs MD simulations of the MOR-MOR homodimer, constructed via both the TM 5/6 (not interacting with Gal_1R) and TM 4/5 (interacting with Gal_1R) interfaces, in complex with Gi (see Methods and fig. S10). These simulations showed that, in contrast to the TM 5/6 interface, TM 5 of the active Gi-bound protomer moved the extracellular part of TM 5 inward in the TM 4/5 interface. Importantly, this movement of TM 5 relocated the position of the key $V238^{5.42}$ (fig. S10). Fig. 4O, P summarizes these findings. In the TM 5/6 interface (Fig. 4O), $W295^{6.48}$ is only partially restricted (depicted as flexible ellipses) by the phenyl ring of (S)-MTD because the dynamic behavior of the ligand is not fully constrained by the partner protomer (depicted as flexible arrows). In contrast, in the TM 4/5 interface (Fig. 4P), the inward movement of $V238^{5.42}$ fully constrained (depicted as a single arrow) the phenyl ring of (S)-MTD, maintaining $W295^{6.48}$ in the inactive conformation (depicted as a single ellipse).

Discussion

(R,S)-MTD is a DEA Schedule II controlled medication with known abuse liability that is prescribed for pain management and treatment of OUD. However, the individual contributions of its enantiomers to its abuse liability and clinical efficacy are not well understood. We found that both (R)-MTD and (S)-MTD produced full agonistic effects on analgesia but only (R)-MTD was reliably self-administered. These findings are in agreement with results from recent studies indicating that (S)-MTD does not lead to reinforcing effects, physical dependence nor withdrawal signs in rats[40] and that it lacks opioid effects, or withdrawal signs and symptoms in humans[5], suggesting that the abuse liability of (R,S)-MTD is mediated by (R)-MTD and not by (S)-MTD. Indeed, our data indicate that (S)-MTD can attenuate the abuse liability of (R)-MTD under some conditions.

Although some experimental and clinical effects of (S)-MTD have been attributed to its NMDAR antagonism[5, 7–9, 41], we demonstrate here that, at pharmacologically relevant doses, (S)-MTD does not interact with NMDARs *in vivo.* Instead, (S)-MTD significantly occupies MORs at doses that promote the classical behavioral effects of opioids in rats: analgesia, catalepsy, and hypothermia. For example, the effective dose at which (S)-MTD produced analgesia is within the range of doses used to produce antidepressant-like effects in rats [6, 7]. For both (R)-MTD and (S)-MTD, the predicted free brain concentrations coincided with their *in vitro* MOR affinities as well as their capacity to selectively occupy MORs *in vivo*. In contrast, we failed to detect *in vivo* NMDAR occupancy at the same doses where MOR occupancy was observed. Therefore, we can conclude that (S)-MTD selectively binds MORs at brain concentrations relevant to its analgesic and antidepressant-like efficacy. Thus, the currently assumed role of NMDAR blockade in the antidepressant effects of (S)-MTD should be reframed in the context of its MOR agonistic properties.

We demonstrated that (S)-MTD does not promote activation of the dopaminergic system despite its agonism of MOR. This lack of effect is likely due to the inability of (S)-MTD to activate MOR-Gal_1R in the VTA, previously shown to mediate the dopaminergic effects

of opioids[16]. On the other hand, (R)-MTD promoted a significantly stronger activation of the VTA dopaminergic system than the reported effect of (R,S)-MTD[16]. The specific lack of effect of (S)-MTD was due to its loss of intrinsic efficacy for MOR-Gal_1R, which also explains its antagonism of (R)-MTD-induced effects in the VTA including dopamine release, [^{35}S]GTPγS recruitment, and locomotor activation. This is the first time to our knowledge that enantiomers have been shown to work in direct opposition at the same pharmacological target.

The significant analgesic and cataleptic effects of (S)-MTD indicate dopamine-independent mechanisms, not mediated by MOR-Gal_1R. As opposed to neuroleptic-induced catalepsy, opioids do not induce catalepsy by inhibiting striatal dopaminergic neurotransmission, but possibly by inhibiting the MOR-expressing striatal and pallidal GABAergic neurons that project to the output structures of the basal ganglia[30, 42, 43]. These two functionally opposite MOR-dependent effects, locomotor activation and catalepsy, are both present but differentially dominate in mice and rats, respectively. In fact, locomotor activation can also be elicited in rats with the intracranial injection of opioids in the VTA[44], and catalepsy has been reported with relatively high doses of opioids in mice[45] and likely contributes to the descending limb of the dose response curve for opioid-induced locomotor activity in mice[26, 28].

The question of whether dopamine neurotransmission underlies the reinforcing properties of opioids has been a matter of debate[46–48]. Nevertheless, results from chemogenetic and optogenetic experiments in mice[49] strongly support the involvement of VTA dopamine neurons projecting to the ventral striatum in driving heroin reinforcement. The present results showing IVSA of (R,S)-MTD and (R)-MTD but not (S)-MTD, are consistent with the dopaminergic hypothesis. Nevertheless, at high doses, (S)-MTD was able to substitute for (R)-MTD in rats trained on (R)-MTD, which support the involvement of additional non-dopaminergic mechanisms in opioid reinforcement. Importantly, the dose response of (R,S)-MTD IVSA was qualitatively different from that of (R)-MTD, with a significantly higher peak and a pronounced shift to the right. This could be explained by (S)-MTD counteracting the effect of (R)-MTD at sufficiently high doses of (R,S)-MTD.

One potential adverse effect of (R,S)-MTD use is that it can cause cardiac arrythmia[50]. This has been attributed to high concentrations of the drug and perhaps to the presence of (S)-MTD, which one study reported blocks the Ether-à-go-go-Related Gene 1 (hERG) channel 3.5-fold more potently than (R)-MTD[51]. However, the stereoselective contribution of (R,S)-MTD enantiomers to these effects has been challenged[52]. We did not observe any meaningful binding for (R)-MTD or (S)-MTD at hERG, even at a concentration of 10 μM. Furthermore, recent clinical studies assessing (S)-MTD for depression have not reported any cardiac arrythmias[9]. It is therefore unclear to what extent (S)-MTD contributes to the cardiac effects of (R,S)-MTD.

Combined, the present results help explain the clinical profile of (R,S)-MTD, since they indicate that its lower abuse liability, as compared with other opioids[16, 53], are due to the specific effect of (S)-MTD at MOR-Gal_1R heteromers which counteract rewarding and dopamine releasing effects of (R)-MTD. In addition, the results suggest that the separation

of reinforcing vs. therapeutic effects of (R,S)-MTD[16] should be significantly augmented with (S)-MTD. (S)-MTD could then be used clinically as analgesic, antidepressant, or for the treatment of opioid withdrawal or restless legs syndrome, with the anticipation of low abuse liability. The results of the *in silico* analysis provide information about the possible molecular mechanism underlying MOR-Gal_1R heteromer-dependent pharmacodynamic properties of (S)-MTD, which could also guide the search for novel (S)-MTD-like therapeutics.

Supplementary Material

Refer to Web version on PubMed Central for supplementary material.

Acknowledgements

We thank Shelley Jackson, PhD and Lindsay Kryszak from the Translational Analytical Core at NIDA. We also than Rik Kline, PhD from the Chemistry and Pharmaceutics Branch and the NIDA Drug Supply Program and David White, PhD from the Medications Discovery and Toxicology Branch at NIDA.

Funding

This work was supported by the intramural funds of the National Institute on Drug Abuse (ZIA DA000493, ZIA DA000069, ZIA DA000522); grant PID2020-113938RB-I00 (N.L., V.C.-A., E.M., V.C.), PID2022-140912OB-I00 (L.P.), and Juan de la Cierva fellowship FJC2019-041020-I (V.C.-A.) from the Spanish MCIN/AEI/ 10.13039/501100011033; “Generalitat de Catalunya”, Spain, grant 2021-SGR-00230 (N.L., E.M., V.C.). D Weinshenker was supported by extramural funding from NIDA (DA049257).

Data Availability

The datasets generated during and/or analyzed during the current study are available from the corresponding author on reasonable request.

References

1. Dole VP, Nyswander M. A Medical Treatment for Diacetylmorphine (Heroin) Addiction. A Clinical Trial with Methadone Hydrochloride. Jama 1965; 193: 646–650. [PubMed: 14321530]
2. Salsitz E, Wiegand T. Pharmacotherapy of Opioid Addiction: “Putting a Real Face on a False Demon”. J Med Toxicol 2016; 12(1): 58–63. [PubMed: 26567033]
3. Chem KK. Pharmacology of methadone and related compounds. Ann N Y Acad Sci 1948; 51(Art 1): 83–97. [PubMed: 18890119]
4. Casati A, Piontek D, Pfeiffer-Gerschel T. Patterns of non-compliant buprenorphine, levomethadone, and methadone use among opioid dependent persons in treatment. Subst Abuse Treat Prev Policy 2014; 9: 19. [PubMed: 24885218]
5. Fava M, Stahl S, Pani L, De Martin S, Pappagallo M, Guidetti C et al. REL-1017 (Esmethadone) as Adjunctive Treatment in Patients With Major Depressive Disorder: A Phase 2a Randomized Double-Blind Trial. The American journal of psychiatry 2022; 179(2): 122–131. [PubMed: 34933568]
6. Fogaca MV, Fukumoto K, Franklin T, Liu RJ, Duman CH, Vitolo OV et al. N-Methyl-D-aspartate receptor antagonist d-methadone produces rapid, mTORC1-dependent antidepressant effects. Neuropsychopharmacology 2019; 44(13): 2230–2238. [PubMed: 31454827]
7. Hanania T, Manfredi P, Inturrisi C, Vitolo OV. The N-methyl-D-aspartate receptor antagonist d-methadone acutely improves depressive-like behavior in the forced swim test performance of rats. Exp Clin Psychopharmacol 2020; 28(2): 196–201. [PubMed: 31368772]

8. De Martin S, Gabbia D, Folli F, Bifari F, Fiorina P, Ferri N et al. REL-1017 (Esmethadone) Increases Circulating BDNF Levels in Healthy Subjects of a Phase 1 Clinical Study. Front Pharmacol 2021; 12: 671859. [PubMed: 33995104]
9. Bernstein G, Davis K, Mills C, Wang L, McDonnell M, Oldenhof J et al. Characterization of the Safety and Pharmacokinetic Profile of D-Methadone, a Novel N-Methyl-D-Aspartate Receptor Antagonist in Healthy, Opioid-Naive Subjects: Results of Two Phase 1 Studies. J Clin Psychopharmacol 2019; 39(3): 226–237. [PubMed: 30939592]
10. Gorman AL, Elliott KJ, Inturrisi CE. The d- and l-isomers of methadone bind to the non-competitive site on the N-methyl-D-aspartate (NMDA) receptor in rat forebrain and spinal cord. Neuroscience letters 1997; 223(1): 5–8. [PubMed: 9058409]
11. Williams NR, Heifets BD, Blasey C, Sudheimer K, Pannu J, Pankow H et al. Attenuation of Antidepressant Effects of Ketamine by Opioid Receptor Antagonism. The American journal of psychiatry 2018; 175(12): 1205–1215. [PubMed: 30153752]
12. Bonaventura J, Lam S, Carlton M, Boehm MA, Gomez JL, Solis O et al. Pharmacological and behavioral divergence of ketamine enantiomers: implications for abuse liability. Molecular psychiatry 2021; 26(11): 6704–6722. [PubMed: 33859356]
13. Klein ME, Chandra J, Sheriff S, Malinow R. Opioid system is necessary but not sufficient for antidepressive actions of ketamine in rodents. Proc Natl Acad Sci U S A 2020; 117(5): 2656–2662. [PubMed: 31941713]
14. Levinstein MR, Carlton ML, Di Ianni T, Ventriglia EN, Rizzo A, Gomez JL et al. Mu opioid receptor activation mediates (S)-ketamine reinforcement in rats: implications for abuse liability. Biol Psychiatry 2023; 93(12): 1118–1126. [PubMed: 36841701]
15. Kristensen K, Christensen CB, Christrup LL. The mu1, mu2, delta, kappa opioid receptor binding profiles of methadone stereoisomers and morphine. Life Sci 1995; 56(2): PL45–50. [PubMed: 7823756]
16. Cai NS, Quiroz C, Bonaventura J, Bonifazi A, Cole TO, Purks J et al. Opioid-galanin receptor heteromers mediate the dopaminergic effects of opioids. J Clin Invest 2019; 129(7): 2730–2744. [PubMed: 30913037]
17. Spiga R, Grabowski J, Silverman PB, Meisch RA. Human methadone self-administration: effects of dose and ratio requirement. Behavioural pharmacology 1996; 7(2): 130–137. [PubMed: 11224404]
18. Martin TJ, Kim SA, Buechler NL, Porreca F, Eisenach JC. Opioid self-administration in the nerve-injured rat: relevance of antiallodynic effects to drug consumption and effects of intrathecal analgesics. Anesthesiology 2007; 106(2): 312–322. [PubMed: 17264726]
19. Steinpreis RE, Rutell AL, Parrett FA. Methadone produces conditioned place preference in the rat. Pharmacol Biochem Behav 1996; 54(2): 339–341. [PubMed: 8743593]
20. O'Connor EC, Chapman K, Butler P, Mead AN. The predictive validity of the rat self-administration model for abuse liability. Neurosci Biobehav Rev 2011; 35(3): 912–938. [PubMed: 21036191]
21. Smith DA, Di L, Kerns EH. The effect of plasma protein binding on in vivo efficacy: misconceptions in drug discovery. Nat Rev Drug Discov 2010; 9(12): 929–939. [PubMed: 21119731]
22. Kalvass JC, Maurer TS, Pollack GM. Use of plasma and brain unbound fractions to assess the extent of brain distribution of 34 drugs: comparison of unbound concentration ratios to in vivo p-glycoprotein efflux ratios. Drug Metab Dispos 2007; 35(4): 660–666. [PubMed: 17237155]
23. Holm KM, Linnet K. Determination of the unbound fraction of R- and S-methadone in human brain. Int J Legal Med 2016; 130(6): 1519–1526. [PubMed: 27055456]
24. Allouche S, Noble F, Marie N. Opioid receptor desensitization: mechanisms and its link to tolerance. Front Pharmacol 2014; 5: 280. [PubMed: 25566076]
25. Finn AK, Whistler JL. Endocytosis of the mu opioid receptor reduces tolerance and a cellular hallmark of opiate withdrawal. Neuron 2001; 32(5): 829–839. [PubMed: 11738029]
26. Brase DA, Loh HH, Way EL. Comparison of the effects of morphine on locomotor activity, analgesia and primary and protracted physical dependence in six mouse strains. The Journal of pharmacology and experimental therapeutics 1977; 201(2): 368–374. [PubMed: 558328]

27. Kuschinsky K, Hornykiewicz O. Effects of morphine on striatal dopamine metabolism: possible mechanism of its opposite effect on locomotor activity in rats and mice. European journal of pharmacology 1974; 26(1): 41–50. [PubMed: 4598755]
28. Middaugh LD, Kapetanovic IM, Sweeney DJ, Ingram DK. Methadone in brain and its effects on locomotor activity of young and aged mice. Neurobiol Aging 1983; 4(4): 321–326. [PubMed: 6672639]
29. Tzschentke TM, Schmidt WJ. Morphine-induced catalepsy is augmented by NMDA receptor antagonists, but is partially attenuated by an AMPA receptor antagonist. European journal of pharmacology 1996; 295(2–3): 137–146. [PubMed: 8720577]
30. Costall B, Naylor RJ. On catalepsy and catatonia and the predictability of the catalepsy test for neuroleptic activity. Psychopharmacologia 1974; 34(3): 233–241. [PubMed: 4594816]
31. Zarrindast MR, Zarghi A. Morphine stimulates locomotor activity by an indirect dopaminergic mechanism: possible D-1 and D-2 receptor involvement. Gen Pharmacol 1992; 23(6): 1221–1225. [PubMed: 1362552]
32. Chefer VI, Kieffer BL, Shippenberg TS. Basal and morphine-evoked dopaminergic neurotransmission in the nucleus accumbens of MOR- and DOR-knockout mice. The European journal of neuroscience 2003; 18(7): 1915–1922. [PubMed: 14622224]
33. Hnasko TS, Sotak BN, Palmiter RD. Morphine reward in dopamine-deficient mice. Nature 2005; 438(7069): 854–857. [PubMed: 16341013]
34. Matsui A, Jarvie BC, Robinson BG, Hentges ST, Williams JT. Separate GABA afferents to dopamine neurons mediate acute action of opioids, development of tolerance, and expression of withdrawal. Neuron 2014; 82(6): 1346–1356. [PubMed: 24857021]
35. Santos EJ, Banks ML, Negus SS. Role of Efficacy as a Determinant of Locomotor Activation by Mu Opioid Receptor Ligands in Female and Male Mice. J Pharmacol Exp Ther 2022; 382(1): 44–53. [PubMed: 35489781]
36. Vezina P, Kalivas PW, Stewart J. Sensitization occurs to the locomotor effects of morphine and the specific mu opioid receptor agonist, DAGO, administered repeatedly to the ventral tegmental area but not to the nucleus accumbens. Brain Res 1987; 417(1): 51–58. [PubMed: 3040185]
37. De Oliveira PA, Moreno E, Casajuana-Martin N, Casado-Anguera V, Cai NS, Camacho-Hernandez GA et al. Preferential Gs protein coupling of the galanin Gal(1) receptor in the micro-opioid-Gal(1) receptor heterotetramer. Pharmacol Res 2022; 182: 106322. [PubMed: 35750299]
38. Zhuang Y, Wang Y, He B, He X, Zhou XE, Guo S et al. Molecular recognition of morphine and fentanyl by the human mu-opioid receptor. Cell 2022; 185(23): 4361–4375 e4319. [PubMed: 36368306]
39. Huang W, Manglik A, Venkatakrishnan AJ, Laeremans T, Feinberg EN, Sanborn AL et al. Structural insights into μ-opioid receptor activation. Nature 2015; 524(7565): 315–321. [PubMed: 26245379]
40. Henningfield J, Gauvin D, Bifari F, Fant R, Shram M, Buchhalter A et al. REL-1017 (esmethadone; D-methadone) does not cause reinforcing effect, physical dependence and withdrawal signs in Sprague Dawley rats. Sci Rep 2022; 12(1): 11389. [PubMed: 35794162]
41. Holtman JR, Jr., Wala EP. Characterization of the antinociceptive and pronociceptive effects of methadone in rats. Anesthesiology 2007; 106(3): 563–571. [PubMed: 17325516]
42. Moroni F, Cheney DL, Peralta E, Costa E. Opiate receptor agonists as modulators of gamma-aminobutyric acid turnover in the nucleus caudatus, globus pallidus and substantia nigra of the rat. The Journal of pharmacology and experimental therapeutics 1978; 207(3): 870–877. [PubMed: 215744]
43. Turski L, Havemann U, Kuschinsky K. The role of the substantia nigra in motility of the rat. Muscular rigidity, body asymmetry and catalepsy after injection of morphine into the nigra. Neuropharmacology 1983; 22(9): 1039–1048. [PubMed: 6685231]
44. Zangen A, Ikemoto S, Zadina JE, Wise RA. Rewarding and psychomotor stimulant effects of endomorphin-1: anteroposterior differences within the ventral tegmental area and lack of effect in nucleus accumbens. The Journal of neuroscience : the official journal of the Society for Neuroscience 2002; 22(16): 7225–7233. [PubMed: 12177217]

45. VanderWende C, Spoerlein MT. Morphine-induced catalepsy in mice. Modification by drugs acting on neurotransmitter systems. Neuropharmacology 1979; 18(7): 633–637. [PubMed: 40155]
46. Badiani A, Belin D, Epstein D, Calu D, Shaham Y. Opiate versus psychostimulant addiction: the differences do matter. Nat Rev Neurosci 2011; 12(11): 685–700. [PubMed: 21971065]
47. Blum K, Thanos PK, Oscar-Berman M, Febo M, Baron D, Badgaiyan RD et al. Dopamine in the Brain: Hypothesizing Surfeit or Deficit Links to Reward and Addiction. J Reward Defic Syndr 2015; 1(3): 95–104. [PubMed: 27398406]
48. Nutt DJ, Lingford-Hughes A, Erritzoe D, Stokes PR. The dopamine theory of addiction: 40 years of highs and lows. Nat Rev Neurosci 2015; 16(5): 305–312. [PubMed: 25873042]
49. Corre J, van Zessen R, Loureiro M, Patriarchi T, Tian L, Pascoli V et al. Dopamine neurons projecting to medial shell of the nucleus accumbens drive heroin reinforcement. Elife 2018; 7.
50. Grilo LS, Carrupt PA, Abriel H. Stereoselective Inhibition of the hERG1 Potassium Channel. Front Pharmacol 2010; 1: 137. [PubMed: 21833176]
51. Eap CB, Crettol S, Rougier JS, Schlapfer J, Sintra Grilo L, Deglon JJ et al. Stereoselective block of hERG channel by (S)-methadone and QT interval prolongation in CYP2B6 slow metabolizers. Clin Pharmacol Ther 2007; 81(5): 719–728. [PubMed: 17329992]
52. Andrassy G, Szabo A. Methadone-induced QTc prolongation: is it due to stereoselective block of hERG or to inappropriate QT interval correction? Clin Pharmacol Ther 2008; 83(5): 671; author reply 672. [PubMed: 18043689]
53. Maxwell JC, McCance-Katz EF. Indicators of buprenorphine and methadone use and abuse: what do we know? The American journal on addictions / American Academy of Psychiatrists in Alcoholism and Addictions 2010; 19(1): 73–88.
54. Vandeputte MM, Krotulski AJ, Walther D, Glatfelter GC, Papsun D, Walton SE et al. Pharmacological evaluation and forensic case series of N-pyrrolidino etonitazene (etonitazepyne), a newly emerging 2-benzylbenzimidazole 'nitazene' synthetic opioid. Arch Toxicol 2022; 96(6): 1845–1863. [PubMed: 35477798]
55. Berhane I, Hin N, Thomas AG, Huang Q, Zhang C, Veeravalli V et al. Thieno[2,3-d]pyrimidine-Based Positive Allosteric Modulators of Human Mas-Related G Protein-Coupled Receptor X1 (MRGPRX1). J Med Chem 2022; 65(4): 3218–3228. [PubMed: 35119273]
56. Bergh MS, Bogen IL, Garibay N, Baumann MH. Pharmacokinetics and pharmacodynamics of cyclopropylfentanyl in male rats. Psychopharmacology (Berl) 2021; 238(12): 3629–3641. [PubMed: 34613431]
57. Wong B, Perkins MW, Tressler J, Rodriguez A, Devorak J, Sciuto AM. Effects of inhaled aerosolized carfentanil on real-time physiological responses in mice: a preliminary evaluation of naloxone. Inhal Toxicol 2017; 29(2): 65–74. [PubMed: 28330429]
58. Anden NE, Grabowska-Anden M. Stimulation of D1 dopamine receptors reveals direct effects of the preferential dopamine autoreceptor agonist B-HT 920 on postsynaptic dopamine receptors. Acta Physiol Scand 1988; 134(2): 285–290. [PubMed: 2852446]
59. Casado V, Ferrada C, Bonaventura J, Gracia E, Mallol J, Canela EI et al. Useful pharmacological parameters for G-protein-coupled receptor homodimers obtained from competition experiments. Agonist-antagonist binding modulation. Biochem Pharmacol 2009; 78(12): 1456–1463. [PubMed: 19643089]
60. Huang J, Chen S, Zhang JJ, Huang XY. Crystal structure of oligomeric beta1-adrenergic G protein-coupled receptors in ligand-free basal state. Nat Struct Mol Biol 2013; 20(4): 419–425. [PubMed: 23435379]
61. Manglik A, Kruse AC, Kobilka TS, Thian FS, Mathiesen JM, Sunahara RK et al. Crystal structure of the μ-opioid receptor bound to a morphinan antagonist. Nature 2012; 485(7398): 321–326. [PubMed: 22437502]
62. Schott-Verdugo S, Gohlke H. PACKMOL-Memgen: A Simple-To-Use, Generalized Workflow for Membrane-Protein-Lipid-Bilayer System Building. J Chem Inf Model 2019; 59(6): 2522–2528. [PubMed: 31120747]
63. Abraham MJ, Murtola T, Schulz R, Páll S, Smith JC, Hess B et al. GROMACS: High performance molecular simulations through multi-level parallelism from laptops to supercomputers. SoftwareX 2015; 1–2: 19–25.

64. Navarro G, Gonzalez A, Campanacci S, Rivas-Santisteban R, Reyes-Resina I, Casajuana-Martin N et al. Experimental and computational analysis of biased agonism on full-length and a C-terminally truncated adenosine A(2A) receptor. Comput Struct Biotechnol J 2020; 18: 2723–2732. [PubMed: 33101610]

65. Michaud-Agrawal N, Denning EJ, Woolf TB, Beckstein O. MDAnalysis: a toolkit for the analysis of molecular dynamics simulations. J Comput Chem 2011; 32(10): 2319–2327. [PubMed: 21500218]

66. Lomize MA, Pogozheva ID, Joo H, Mosberg HI, Lomize AL. OPM database and PPM web server: resources for positioning of proteins in membranes. Nucleic Acids Res 2012; 40(Database issue): D370–376. [PubMed: 21890895]

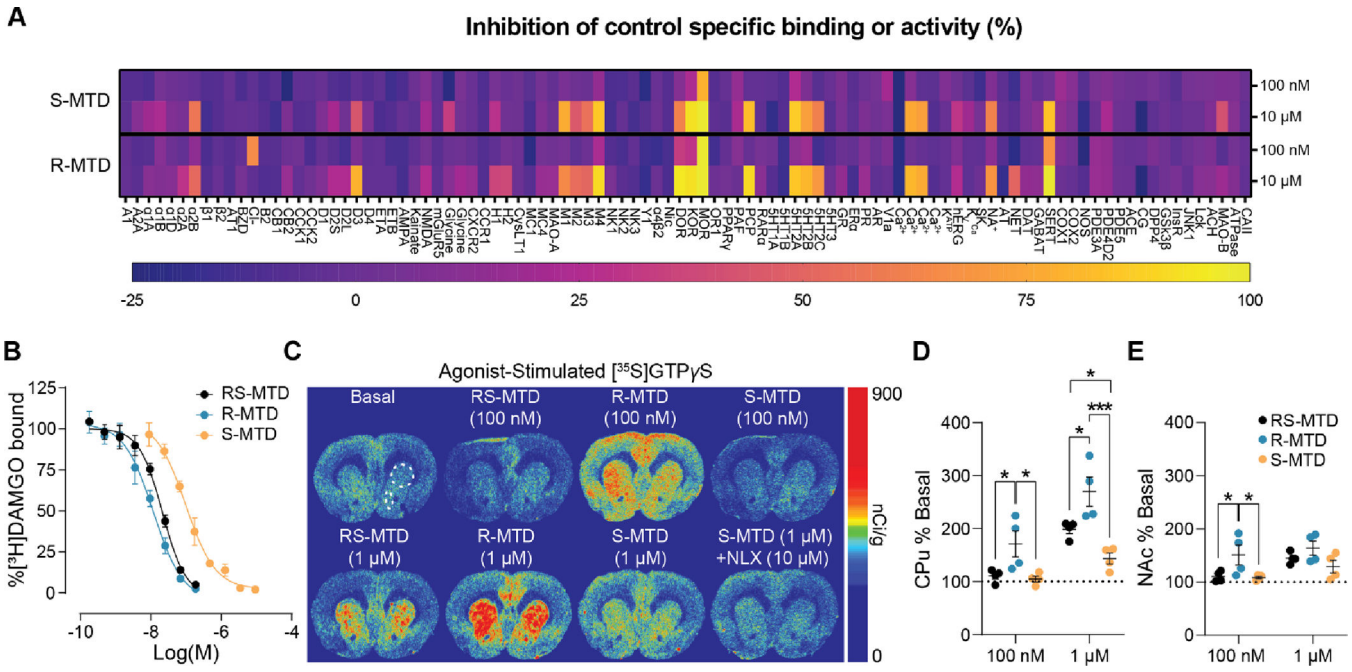

Fig. 1. Methadone and its enantiomers are MOR agonists.

A, Receptor and enzyme competitive screen at two concentrations (100 nM and 10 μM) of (S)- and (R)-MTD. **B,** Competition binding assays of (S)-MTD (orange), (R)-MTD (blue), or (R,S)-MTD (black) versus [^{3}H]DAMGO. **C-E,** Representative slices (**C**) and analysis from methadone-stimulated [^{35}S]GTPγS autoradiography for CPu (**D**, upper circle) and NAc (**E**, lower ellipse). Values are shown as mean ± standard error of the mean. CPu = caudate putamen; MOR = mu opioid receptor; MTD = methadone; NLX = naloxone; NAc = nucleus accumbens. *$P < 0.05$, **$P < 0.01$, ***$P < 0.001$.

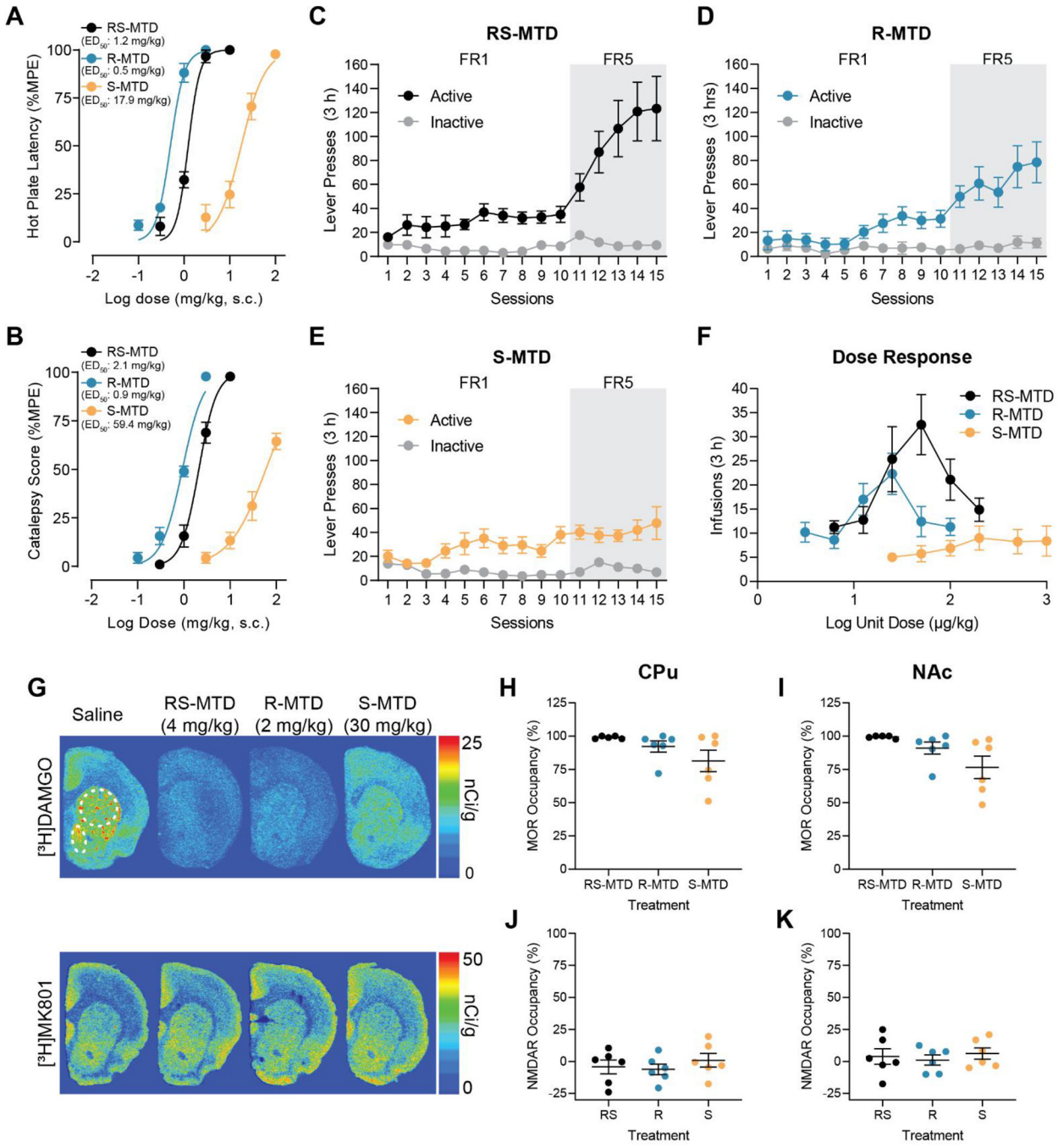

Fig 2. Analgesic, cataleptic and differential abuse liability profile of (R,S)-MTD, (R)-MTD, and (S)-MTD.

A-B, Dose response curves of hotplate latency (**A**) and catalepsy (**B**) for (R,S)-MTD (black), (R)-MTD (blue) and (S)-MTD (orange). **C-E,** Lever presses during IVSA training for (R,S)-MTD (100 µg/kg/infusion, **C**), (R)-MTD (50 µg/kg/infusion, **D**), and (S)-MTD (500 µg/kg/infusion, **E**). **F,** IVSA dose responses for (R,S)-MTD, (R)-MTD, and (S)-MTD. **G-K,** Representative slices (**G**) and analysis of receptor occupancy by (R,S)-MTD, (R)-MTD, or (S)-MTD of MORs ([^{3}H]DAMGO, 5nM) in CPU (**H**, upper circle) and NAc (**i**, lower

ellipse) or NMDARs ([^{3}H]MK-801, 5nM) (**J-K**). Values are shown as mean ± standard error of the mean. CPu = caudate putamen; ED_{50} = half maximal effective dose; FR = fixed-ratio schedule; IVSA = intravenous self-administration; MOR = μ opioid receptor; MPE = maximum possible effect; MTD = methadone; NAc = nucleus accumbens; NMDAR = N-methyl-D-aspartate receptor.

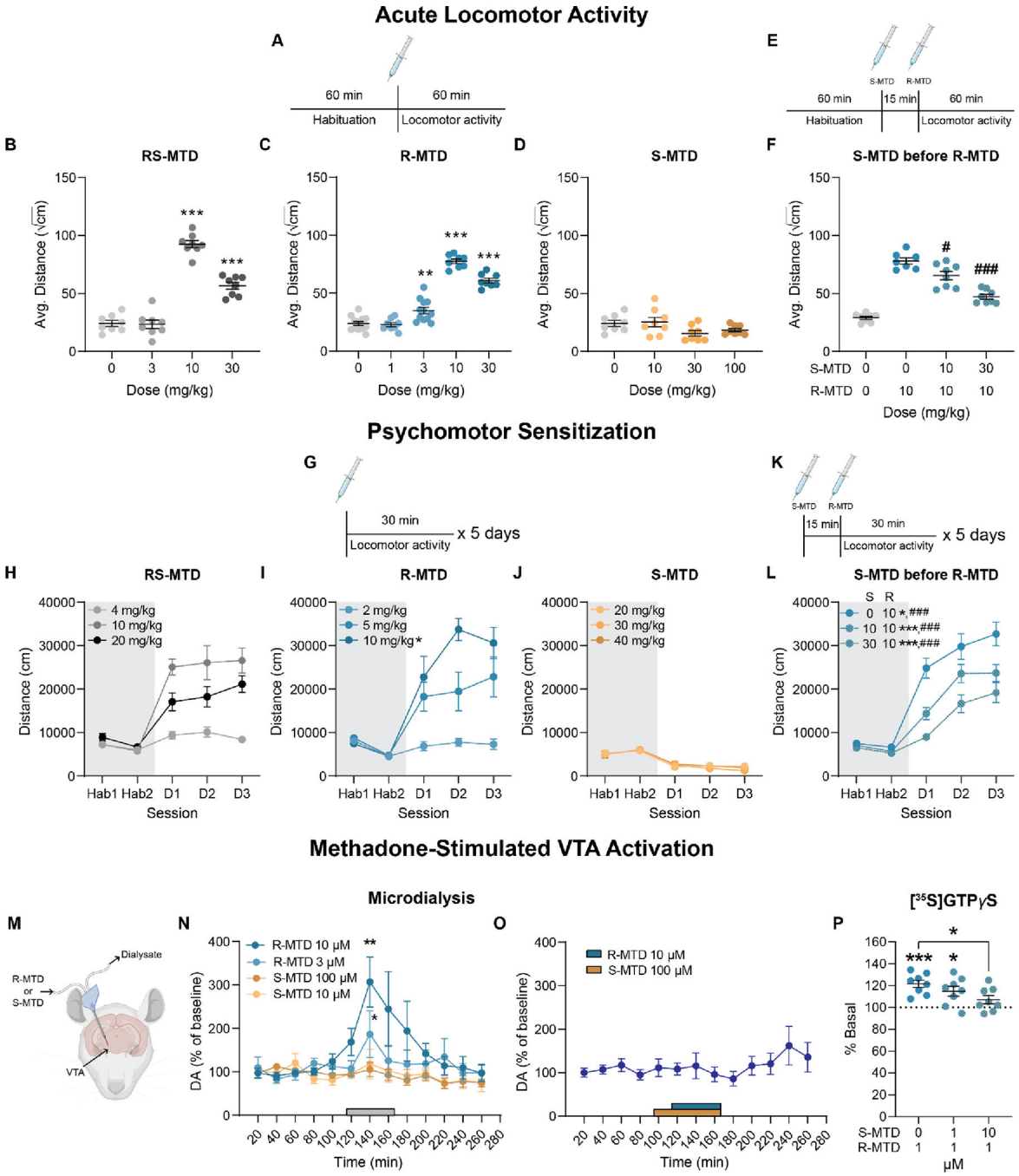

Fig. 3. VTA-dependent neurochemical and behavioral effects of (R)-MTD and (S)-MTD.

Created with BioRender.com. **A-F,** acute locomotor activation schematics (**A, E**) and analysis with (R,S)-MTD (**B**), (R)-MTD (**C**), or (S)-MTD (**D**) alone, or pretreatment of (S)-MTD before (R)-MTD (**F**). Data shown as the average of the square root of centimeters traveled per ten minutes. Asterisks are compared to saline; pound symbols are compared to (R)-MTD alone. **G-L,** psychomotor sensitization schematics (**G, K**) and analysis with (R,S)-MTD (**H**), (R)-MTD (**i**), or (S)-MTD alone (**J**), or pretreatment of (S)-MTD before (R)-MTD (**L**). Asterisks are comparison between D1 and D2; pound symbols are comparison

between D1 and D3. **M-O,** effect of intracranial perfusion of (R)-MTD and (S)-MTD in the VTA on somato-dendritic dopamine release from *in vivo* microdialysis experiments. Values represent mean dopamine concentrations as a percentage of baseline ± standard error of the mean (average of 5 samples before the enantiomer administration). The rectangles in the x axis indicate the period of corresponding enantiomer perfusion. In **O**, co-perfusion of both enantiomers, with (S)-MTD (100 μM) beginning 20 min before (R)-MTD (10 μM). **P,** Analysis of [^{35}S]GTPγS recruitment by R-MTD (1 μM) with or without preincubation of S-MTD (1 μM or 10 μM) in the VTA. Values are shown as mean ± standard error of the mean. D1, 2, 3 = day 1, 2, or 3; Hab = habituation, MTD = methadone, VTA = ventral tegmental area. *,$^{\#}$ $P < 0.05$, **$P < 0.01$, ***,$^{\#\#\#}P < 0.001$.

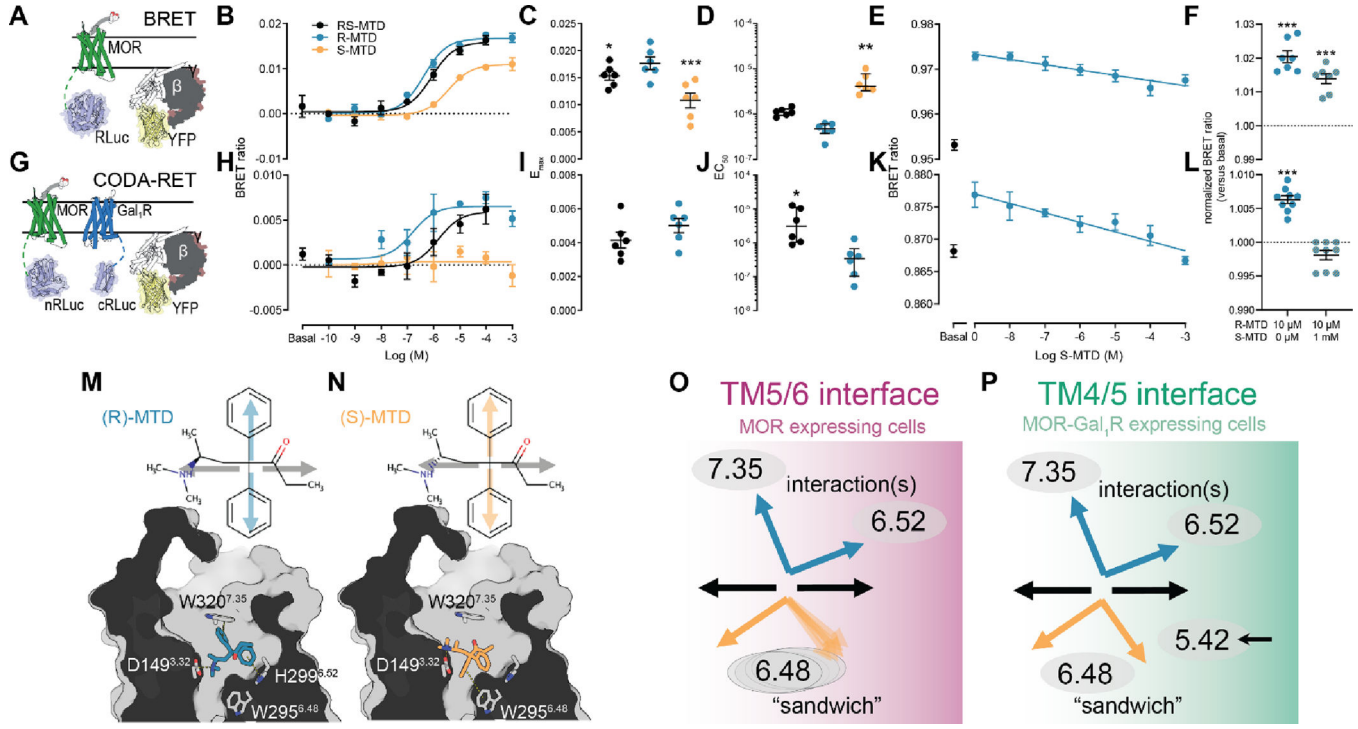

Fig. 4. MOR-Gal$_1$R heteromer-dependent loss of efficacy of (S)-MTD.

A-F, BRET experiments in HEK-293T cells cotransfected with MOR fused to RLuc and the α subunit of the Gi protein fused to YFP (schematically shown in **A**). **G-L.** CODA-RET experiments in HEK-293T cells cotransfected with MOR fused to nRLuc, Gal$_1$R fused to cRLuc and Gi-YFP (schematically shown in **G**). In **B** and **H**, representative experiments with concentration-responses of (R,S)-MTD (black), (R)-MTD (blue), and (S)-MTD (orange); values represent the mean ± standard error of the mean of triplicates; in **C, D, I,** and **J**, corresponding E_{max} and EC_{50} values from 6 independent experiments with triplicates, shown as dots and presented with the mean ± standard error of the mean or median with interquartile ranges, respectively; asterisks are compared to (R)-MTD values. In **E** and **K**, representative experiments of the effect of increasing concentrations of (S)-MTD on BRET and CODA-RET values obtained with (R)-MTD at 100 nM; values represent the mean ± SEM of triplicates; in **F** and **I**, corresponding BRET and CODA-RET values of the effect of (R)-MTD (100 nM) in the presence and absence of (S)-MTD (1 µM) from 7 and 9 independent experiments with triplicates, shown as dots and presented with the mean ± standard error of the mean; asterisks are compared to basal values. **M-N,** Schematic 2D representation of (R)- and (S)-MTD. Grey arrows represent groups of the ligand located toward the conserved protonated amine (left) and toward the -CO-CH2-CH3 moiety (right). The phenyl groups of methadone are depicted by either blue (R-) or orange (S-) arrows. Docking and MD-simulated models (fig. S7) of (R)- and (S)-MTD bound to the MOR. The phenyl rings, in a "V" shaped conformation, point up to interact with H299$^{6.52}$ and W320$^{7.35}$ in (R)-MTD, and point down to interact with W295$^{6.48}$ in (S)-MTD. **O-P**, Previous results[37] show that MOR forms homodimers via the TM 5/6 interface in the absence of Gal$_1$R or via the TM 4/5 interface in the presence of Gal$_1$R. MD simulations show that the TM 4/5 triggers an inward movement of TM 5 and, importantly, the inward

movement of $V238^{5.42}$ (fig. S9). Thus, in the TM 5/6 interface the phenyl ring of (S)-MTD (flexible arrows) partially restricts the conformation of $W295^{6.48}$ (flexible ellipses), whereas in the TM4/5 interface $V238^{5.42}$ restricts the conformation of the phenyl ring (single arrow) and in consequence $W295^{6.48}$ (single ellipse) in the inactive conformation. BRET = bioluminescence resonance energy transfer; CODA-RET = Complemented donor-acceptor resonance energy transfer; E_{max} = maximal response; EC_{50} = half maximal effective concentration; Gal_1R = galanin 1 receptor; MD = molecular dynamics; MOR = mu opioid receptor; MTD = methadone. $*P < 0.05$, $**P < 0.01$, $***P < 0.001$